Atmos. Chem. Phys., 22, 8805–8817, 2022
https://doi.org/10.5194/acp-22-8805-2022

Atmospheric Chemistry and Physics
Open Access
EGU

Viscosity and physical state of sucrose mixed with ammonium sulfate droplets

Rani Jeong[1], Joseph Lilek[2], Andreas Zuend[2], Rongshuang Xu[3], Man Nin Chan[3,4], Dohyun Kim[1], Hi Gyu Moon[5], and Mijung Song[1,6]

[1]Department of Environment and Energy, Jeonbuk National University, Jeonju, Republic of Korea
[2]Department of Atmospheric and Oceanic Sciences, McGill University, Montréal, Quebec, Canada
[3]Earth System Science Programme, Faculty of Science, The Chinese University of Hong Kong, Hong Kong, Hong Kong SAR, China
[4]The Institute of Environment, Energy and Sustainability, The Chinese University of Hong Kong, Hong Kong, Hong Kong SAR, China
[5]Center for Ecological Risk Assessment, Korea Institute of Toxicology (KIT), Jinju 52834, Republic of Korea
[6]Department of Earth and Environmental Sciences, Jeonbuk National University, Jeonju, Republic of Korea

Correspondence: Mijung Song (mijung.song@jbnu.ac.kr)

Received: 28 January 2022 – Discussion started: 7 February 2022
Revised: 16 June 2022 – Accepted: 16 June 2022 – Published: 8 July 2022

Abstract. Although knowledge of the physical state of aerosol particles is essential to understand atmospheric chemistry model and measurements, information on the viscosity and physical state of aerosol particles consisting of organic and inorganic salts is still rare. Herein, we quantified viscosities at 293 ± 1 K upon dehydration for the binary systems, sucrose–H_2O and ammonium sulfate (AS)–H_2O, and the ternary systems, sucrose–AS–H_2O for organic-to-inorganic dry mass ratios (OIRs) = 4 : 1, 1 : 1, and 1 : 4 using bead-mobility and poke-and-flow techniques. Based on the viscosity value of the aerosol particles, we defined the physical states of the total aerosol particles studied in this work. For binary systems, the viscosity of sucrose–H_2O particles gradually increased from $\sim 4 \times 10^{-1}$ to $> \sim 1 \times 10^{8}$ Pa s when the relative humidity (RH) decreased from ∼ 81 % to ∼ 24 %, ranging from liquid to semisolid or solid state, which agrees with previous studies. The viscosity of AS–H_2O particles remained in the liquid state ($< 10^{2}$ Pa s) for RH $> \sim 50$ %, while for RH $\leq \sim 50$ %, the particles showed a viscosity of $> \sim 1 \times 10^{12}$ Pa s, corresponding to a solid state. In case of the ternary systems, the viscosity of organic-rich particles (OIR = 4 : 1) gradually increased from $\sim 1 \times 10^{-1}$ to $\sim 1 \times 10^{8}$ Pa s for a RH decrease from ∼ 81 % to ∼ 18 %, similar to the binary sucrose–H_2O particles. This indicates that the sucrose–AS–H_2O particles range from liquid to semisolid or solid across the RH. In the ternary particles for OIR = 1 : 1, the viscosities ranged from less than $\sim 1 \times 10^{2}$ for RH > 34 % to $> \sim 1 \times 10^{8}$ Pa s at ∼ 27 % RH. The viscosities correspond to liquid for RH $> \sim 34$ %, semisolid for ~ 34 % < RH < ∼ 27 %, and semisolid or solid for RH < ∼ 27 %. Compared to the organic-rich particles, in the inorganic-rich particles (OIR = 1 : 4), drastic enhancement in viscosity was observed as RH decreased; the viscosity increased by approximately 8 orders of magnitude during a decrease in RH from 43 % to 25 %, resulting in liquid to semisolid or solid in the RH range. Overall, all particles studied in this work were observed to exist as a liquid, semisolid, or solid depending on the RH. Furthermore, we compared the measured viscosities of ternary systems with OIRs of 4 : 1, 1 : 1, and 1 : 4 to the predicted viscosities using the Aerosol Inorganic–Organic Mixtures Functional groups Activity Coefficients Viscosity model (AIOMFAC-VISC) predictions with the Zdanovskii–Stokes–Robinson (ZSR) organic–inorganic mixing model, with excellent model–measurement agreement for all OIRs.

1 Introduction

Aerosol particles can play an important role in air quality, climate change, and human health (Kulmala et al., 2011; Zhang et al., 2015; IPCC, 2019; Bhattarai et al., 2020). These aerosol particles comprise mainly organic materials and inorganic salts, which are frequently internally mixed in particles found in the atmosphere (Murphy et al., 2006; Zhang et al., 2007; Jimenez et al., 2009; Wang et al., 2016). Depending on the chemical composition, air temperature, and relative humidity (RH), aerosol particles can undergo liquid–solid and liquid–liquid phase transitions (Martin, 2000; Marcolli, 2014), leading to different physical states. Although such data are useful to inform and validate process models and parameterizations, measurements of various physical states and changes in phase viscosities of mixed organic–inorganic aerosols still remain an understudied area.

Physical states (i.e., liquid, semisolid, and solid) of aerosol particles can be determined from their dynamic viscosities; a viscosity of less than 10^2 Pa s indicates a liquid state, a viscosity between 10^2 and 10^{12} Pa s indicates a semisolid state, and a viscosity of greater than 10^{12} Pa s indicates a solid state (Zobrist et al., 2008; Koop et al., 2011; Kulmala et al., 2011). Most studies of viscosities and the related physical states of aerosol particles have been carried out by means of laboratory studies, because there are almost no direct instruments to quantify the viscosities of ambient, airborne submicron- and supermicron-sized aerosol particles. Numerous laboratory studies on viscosities and physical states undertaken so far have focused on organic aerosols with different types of secondary organic aerosols investigated (Virtanen et al., 2010; Kuwata and Martin, 2012; Perraud et al., 2012; Renbaum-Wolff et al., 2013a; O'brien et al., 2014; Bateman et al., 2015; Song et al., 2015, 2019; M. Song et al., 2016; Song et al., 2021; Athanasiadis et al., 2016; Grayson et al., 2016; Hosny et al., 2016; Yli-Juuti et al., 2017; Ham et al., 2019; Petters et al., 2019; Gervasi et al., 2020). These studies showed that the viscosities of organic aerosol particles can vary depending on RH and chemical composition, leading to different physical states, including amorphous solid (glassy), (semi)solid, and liquid-like phases.

Compared to the number of studies on the viscosity of organic aerosol particles, only a few studies exist for organic compounds mixed with inorganic salts. From laboratory studies, Power et al. (2013) and Rovelli et al. (2019) observed a decrease in viscosity in mixed sucrose–inorganic salt–H_2O particles at a certain RH with an increase in the inorganic fraction of NaCl and $NaNO_3$. Richards et al. (2020b) showed that higher inorganic fraction enhanced organic–inorganic aerosol viscosity at a certain RH due to the ion–molecule interaction. Song et al. (2021) showed that sucrose–$Mg(NO_3)_2$–H_2O and sucrose–$Ca(NO_3)_2$–H_2O particles were present in liquid to semisolid states or even in solid state over the different RH ranges (when probing from high to low RH). From field measurements, Bateman et al. (2017) reported that atmospheric aerosol particles containing organic materials and inorganic salts in central Amazonia are in a nonliquid state with a viscosity greater than 10^2 Pa s even at ~ 95 % RH during pollution events. On the other hand, Liu et al. (2019) observed the phase of ambient aerosol particles in an urban area of China to be in a liquid state at RH greater than 60 %, when the high nitrate fraction was monitored. For a more comprehensive understanding of particle phase viscosities and the related physical states of aerosol particles consisting of a mixture of organic materials and inorganic salts, more datasets are required.

Information of physical states of aerosol particles is critical to understanding heterogeneous reactions between gaseous species and aerosol particles, including the timescales and distinction of possible surface and bulk reactions. Studies have shown that the uptake coefficient of oxidants in the gas phase varied significantly depending on the physical states of involved aerosol particles (Xiao et al., 2011; Slade and Knopf, 2014; Davies and Wilson, 2015; Steimer et al., 2015; Berkemeier et al., 2016; Xu et al., 2020; Lam et al., 2021). For example, Steimer et al. (2015) showed that the ozone uptake coefficient of semisolid particles was approximately 1 order of magnitude less than that of liquid particles. This result can significantly influence the reaction limitation of mass transport.

To get more insights into the viscosities, and related physical states of aerosol particles, we first quantified viscosities of binary mixtures of sucrose–H_2O and ammonium sulfate (AS)–H_2O particles and also ternary mixtures of sucrose–AS–H_2O for organic-to-inorganic dry mass ratios (OIRs) = 4 : 1, 1 : 1, and 1 : 4 under dehydration conditions at 293 ± 1 K. Sucrose was chosen as the model organic substance because it has been investigated as a model surrogate species for secondary organic aerosols (SOAs) in previous studies (Grayson et al., 2016; Y. Song et al., 2016; Rovelli et al., 2019; Song et al., 2021). Moreover, sucrose is a good choice for laboratory studies, because it does not easily crystallize while aqueous particles are dried. AS was used as the model inorganic salt because it has well-defined thermodynamic properties (Braban and Abbatt, 2004; Yeung et al., 2009) and is one of most abundant species in the atmosphere (Zhang et al., 2007; Jimenez et al., 2009). Next, we determined the physical states (i.e., liquid, semisolid, and solid) of the particles as a function of RH based on the viscosity value of the binary and ternary mixtures. In this study, we defined the physical states of the total aerosol particles. Finally, the measured viscosities for sucrose–AS–H_2O droplets with OIRs of 4 : 1, 1 : 1, and 1 : 4 are compared to predictions by the Aerosol Inorganic–Organic Mixtures Functional groups Activity Coefficients Viscosity model (AIOMFAC-VISC) when employing a Zdanovskii–Stokes–Robinson (ZSR) mixing model for viscosity contributions in aqueous organic–inorganic mixtures.

2 Experimental

2.1 Preparation of particles

Sucrose (99.5 % purity, Sigma-Aldrich) and AS (99.9 % purity, Sigma-Aldrich) were dissolved in high-purity water (18 MΩ cm, Merck Millipore Synergy, Germany) to make binary and ternary aqueous mixtures with ∼ 10 wt % solute concentration. Selected OIRs of 4 : 1 (organic-rich), 1 : 1, and 1 : 4 (inorganic-rich) were used for ternary systems. In all experiments, to generate droplets, the solution was sprayed onto a substrate with a hydrophobic coating (Knopf, 2003).

2.2 Determination of viscosity using bead-mobility and poke-and-flow techniques

For viscosity experiments, the substrate containing droplets was placed in a RH-controlled flow cell coupled to an optical microscope (Olympus CKX53 with 40× objective, Japan) (Pant et al., 2006; Ham et al., 2019). During the experiments, RH was continuously monitored using a digital humidity sensor (Sensirion, SHT C3, Switzerland). The uncertainty in the RH was ± 2 %, which was calibrated by observing the deliquescence RH of K_2CO_3 (44 % RH), NaCl (76 % RH), and $(NH_4)_2SO_4$ (80 % RH) at 293 ± 1 K (Winston and Bates, 1960). At the start of the bead-mobility and poke-and-flow experiments, the droplets on a hydrophobic substrate were equilibrated at ∼ 90 % for ∼ 20 min. Subsequently, the RH was decreased to target RH with an equilibrium time of ∼ 30 min for bead-mobility experiment and > ∼ 2 h for poke-and-flow experiments based on the conditioning time of sucrose–H_2O (Grayson et al., 2015). During the experiments, optical morphologies of the particles, 20–100 µm in diameter, were monitored and recorded. All viscosity experiments were conducted at 293 ± 1 K.

The bead-mobility technique has been used to quantify viscosities of aerosol particles in the range of 10^{-3} to 10^3 Pa s (Renbaum-Wolff et al., 2013b; Song et al., 2015; Song et al., 2021). The detailed procedure involved in the bead-mobility technique has been described by previous studies (Renbaum-Wolff et al., 2013a). To outline it briefly, insoluble melamine beads of ∼ 1 µm size (Cat. no. 86296, Sigma-Aldrich) dispersed in pure water were nebulized onto the droplets, which are deposited on a hydrophobic substrate, and the substrate was then mounted in a flow cell as described above. With a total gas flow of ∼ 1200 sccm at target RH at 293 ± 1 K, the gas flow in the flow cell produces a shear stress over the droplet, causing the beads to move. The movements were monitored using an optical microscope and recorded every 1 s using a CCD camera (Hamamatsu, C11440-42U30, Japan). The bead speeds were converted to viscosity using a calibration curve (Fig. S1 in the Supplement), which was derived from bead speeds at different RH versus the known viscosity of the sucrose–H_2O particles at that RH (Fig. S2 in the Supplement). Once the movements became too slow, the poke-and-flow technique was adopted.

The poke-and-flow technique was used in viscosity ranges of > ∼ 10^3 Pa s. This technique has been widely used to determine the phase and viscosity of aerosol particles (Murray et al., 2012; Renbaum-Wolff et al., 2013a; Li et al., 2020; Song et al., 2021). In brief, the particles, which were deposited on a hydrophobic surface and conditioned in a flow cell at target RH as described above, were poked from their top to bottom using a sharp sterile needle (Jung Rim Medical Industrial, South Korea), controlled by a micro-manipulator (Narishige, model MO-152, Japan). The geometrical changes of the particles before, during, and after poking were observed using an optical microscope (Olympus CKX53 with 40× objective, Japan) and recorded using a CCD camera (Hamamatsu, C11440-42U30, Japan).

For particles of sucrose–H_2O and sucrose–AS–H_2O mixtures with an OIR of 4 : 1, a half-torus geometry with an inner hole was observed after poking them at target RH upon dehydration, with the hole then gradually closing to minimize the surface energy. In this case, we measured the experimental flow time ($\tau_{(exp,\ flow)}$), which is the time for the area of the inner hole to reduce to one-fourth of the original hole area, right after poking. Figure S3 in the Supplement shows an example where the $\tau_{(exp,\ flow)}$ of sucrose–H_2O and sucrose–AS–H_2O particles for an OIR of 4 : 1 was measured as 149 s at ∼ 42 % RH and 425 s at 28 % RH. The $\tau_{(exp,\ flow)}$ of each particle was then converted to the lower limit of the viscosity using the equation proposed by Sellier et al. (2015). Details of the process and the measured $\tau_{(exp,\ flow)}$ values are described in Sect. S2 and Fig. S4 in the Supplement, respectively. For particles of AS–H_2O and sucrose–AS–H_2O for OIRs of 1 : 1 and 1 : 4, we could not measure the $\tau_{(exp,\ flow)}$ using the poke-and-flow technique because the droplets were supersaturated with respect to AS upon dehydration.

All particles containing sucrose cracked upon poking at a certain RH, and no detectable material flow was monitored for more than 3 h. Figure 1 presents the optical images of particles containing an organic compound of sucrose that show no inflow or outflow for 3 h after poking. In this case, we determined the lower limit of viscosity as ∼ 1×10^8 Pa s based on previous studies of organic particles (Renbaum-Wolff et al., 2013a; Grayson et al., 2015; Song et al., 2019), though the upper limit to viscosity could not be determined in this study from the poke-and-flow experiments.

2.3 Optical observation of particles during dehydration

To confirm whether the particles studied undergo efflorescence or not during dehydration, particle morphologies were observed optically. The detailed procedure and method have been described in previous studies (Ciobanu et al., 2009; Bertram et al., 2011; Ham et al., 2019). In this study, particles were deposited onto a hydrophobic glass slide (HR3-239, Hampton Research, USA), and then the glass slide was

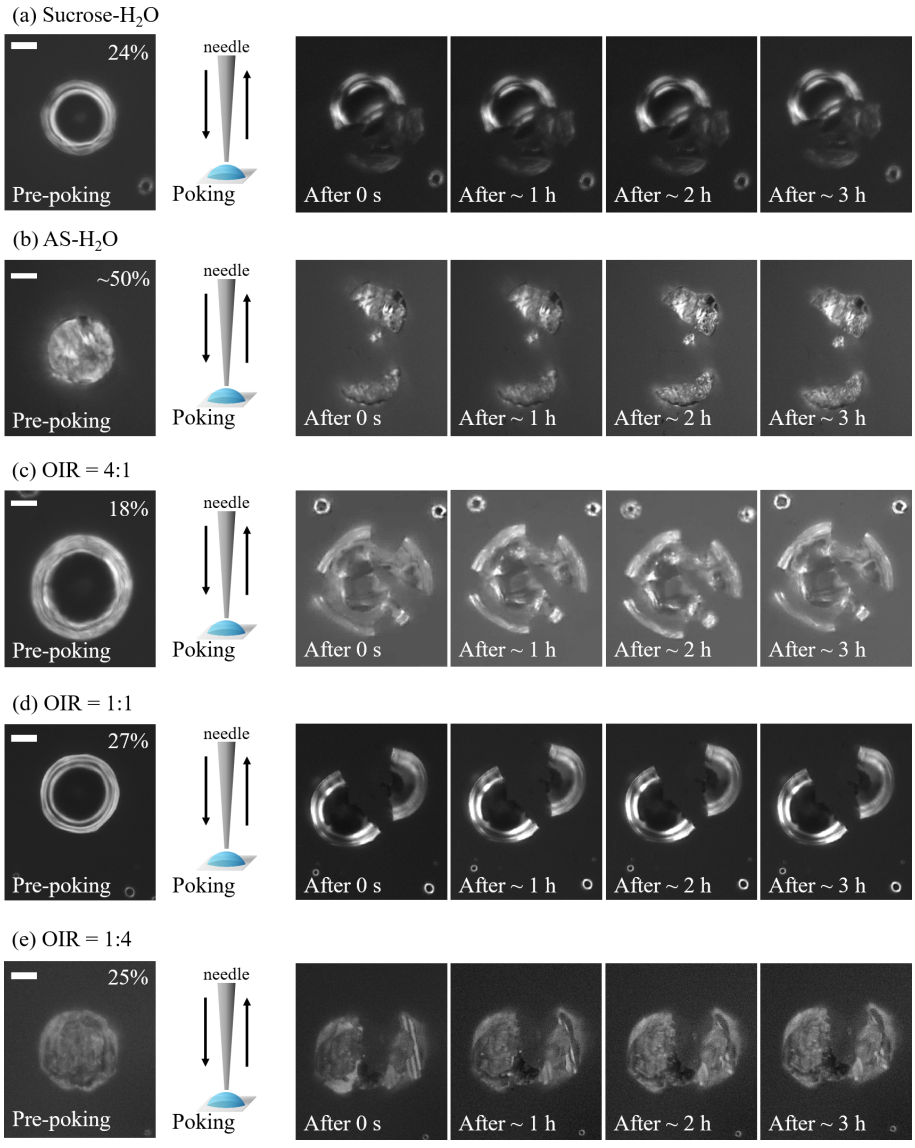

Figure 1. Optical images of particles during poke-and-flow experiments at 293 ± 1 K. When particles cracked at certain relative humidity (RH), they were observed for 3 h, and no restorative flow occurred. During pre-poking, poking, and post-poking process, the RH was maintained. Images are sequentially presented for **(a)** sucrose–H_2O, **(b)** ammonium sulfate (AS)–H_2O, **(c)** sucrose–AS–H_2O particles for organic-to-inorganic dry ratios (OIRs) = 4 : 1, **(d)** sucrose–AS–H_2O particles for OIR = 1 : 1, and (e) sucrose–AS–H_2O particles for OIR = 1 : 4. White scale bar indicates 10 µm.

placed into the flow cell coupled to an optical microscope (Olympus BX43, 40× objective, Japan). During the experiments, RH was decreased from ~ 96 % to ~ 0 % RH at a rate of ~ 0.5 % RH min^{-1} at 290 ± 1 K. RH calibration was carried out in the same way as described in Sect. 2.2, and the RH uncertainty in the cell was ± 1.5 %. The optical images of particles during experiments were recorded every 10 s.

2.4 Thermodynamic calculations

The AIOMFAC model (Zuend et al., 2008, 2011) is a widely used tool for studying aerosol mixing thermodynamics. Equilibrium models based on AIOMFAC can be applied to predict the composition and physical state of aerosol systems (e.g., Zuend and Seinfeld, 2012; Hodas et al., 2015; Bouzidi et al., 2020). This model has been previously used to study mixtures of AS and α-pinene-derived SOA (Zuend and Seinfeld, 2012). The recently integrated viscosity module, AIOMFAC-VISC, can predict the viscosity of aqueous organic mixtures (Gervasi et al., 2020), as well as aqueous electrolyte solutions and aqueous organic–inorganic mixtures (Lilek and Zuend, 2022) using a thermodynamics-based approach, which implies the assumption of a Newtonian fluid behavior.

The AIOMFAC-VISC module consists of separate treatments for mixtures of water with (neutral) organic components and mixtures of water with various inorganic ions. For organic compounds of potentially unknown viscosity, the pure-component viscosities at a given temperature can be estimated based on the glass transition temperatures, T_g, of the components, for example by employing the parameterization introduced by DeRieux et al. (2018) for T_g. This is the default approach in AIOMFAC-VISC. Alternatively, when the (measured) pure-component viscosity or the T_g value is known, it can be used in the model calculation. The temperature-dependent viscosity of pure water is computed based on the parameterization by Dehaoui et al. (2015). With AIOMFAC-VISC, the viscosity of an aqueous organic solution is then predicted via a combinatorial-activity-weighted mixing rule and a residual correction term, as detailed by Gervasi et al. (2020). As was done previously in the study by Song et al. (2021) to obtain the best possible model fit for mixtures containing sucrose, the version of AIOMFAC-VISC used in this work includes a special treatment of H_2O–ether-group interactions in aqueous sucrose solutions.

For mixtures of water with one or more electrolytes, AIOMFAC-VISC uses an equation based on Eyring's absolute rate theory (Glasstone et al., 1941) to calculate viscosity as a function of the Gibbs energy of activation for the volume per mole of mixture and viscous flow. The AIOMFAC-VISC module treating viscosity calculations for electrolyte solutions contains a set of adjustable parameters that have been fitted primarily to bulk viscosity measurements, which do not always agree with droplet-based measurements in the composition range where such measurements overlap (Lilek and Zuend, 2022). Two unique fit parameters are included for each ion species, and one unique parameter is included for each potential cation–anion pair in the mixture. In the case of aqueous AS, the model includes two single-ion parameters for NH_4^+, two parameters for SO_4^{2-}, and one representing specific interaction effects between NH_4^+ and SO_4^{2-}.

AIOMFAC-VISC includes two mixing models for aqueous organic–inorganic mixtures, enabling the coupling of the distinct approaches used for aqueous organic solutions and aqueous electrolyte solutions. The first is called aquelec mixing, wherein all the water contained in the organic–inorganic mixture is assumed to associate with the ions to form an organic-free aqueous electrolyte solution (only used for the purpose of viscosity calculations). This organic-free subsystem effectively replaces pure water in the full system, and the aqueous organic model from Gervasi et al. (2020) is used to calculate the final mixture viscosity. In aquelec, interactions between ions and organics are not included explicitly, although they are partly captured by the ion activity coefficients which are used to calculate the Gibbs energy of activation for viscous flow of the organic-free subsystem. The second mixing model is a ZSR-style approach, wherein the total aerosol water is artificially partitioned between an electrolyte-free aqueous organic subsystem and an organic-free aqueous electrolyte subsystem, which is designed in such a way that dry OIR is preserved. In this mixing model, direct interactions between ions and organics are ignored in the viscosity calculation (indirectly there is an effect since all components affect the water activity of the fully mixed solution, which is matched by the water activities of the subsystems). This has been shown to work reasonably well for non-reactive/non-interacting mixtures but does not work when ions and organic components are interacting strongly to form aggregates of a particular stoichiometry, for example in the gel-forming mixtures described by Richards et al. (2020a, b). Lilek and Zuend (2022) describe further details about the AIOMFAC-VISC method and modeling options for the viscosity of organic–inorganic mixtures.

3 Results and discussion

3.1 Viscosities in binary systems of sucrose–H_2O and AS–H_2O

The viscosity of sucrose–H_2O particles has already been determined by many studies using different techniques at a temperature of 293–297 K (Hosny et al., 2013; Power et al., 2013; Song et al., 2015; Y. Song et al., 2016; Song et al., 2021). In this study, the viscosity of sucrose–H_2O particles gradually increased from $\sim 4 \times 10^{-1}$ to $> \sim 1 \times 10^{8}$ Pa s as RH decreased from $\sim 81\,\%$ to $\sim 24\,\%$ at a temperature of 293 ± 1 K (Fig. 2a). Our result agrees with the results of previous works as shown in Fig. 2a. From the values of viscosity, sucrose–H_2O particles were determined to be in a liquid state for RH greater than $\sim 68\,\%$, a semisolid state for RH values between $\sim 36\,\%$ and $\sim 68\,\%$, and semisolid or even a solid state for RH values less than $\sim 24\,\%$.

Figure 2b also illustrates the RH-dependent viscosities of AS–H_2O particles. The mean viscosities at 293 ± 1 K of AS–H_2O particles determined by the bead-mobility experiment increased from $\sim 2 \times 10^{-2}$ to $\sim 7 \times 10^{-2}$ Pa s for mean RH ranging from $\sim 61\,\%$ to $\sim 50\,\%$ (at $\sim 50\,\%$ RH, we only observed bead movements with non-effloresced particles). This corresponds to a liquid state for RH $> \sim 50\,\%$.

Upon dehydration, AS–H_2O particles effloresced in the RH range between $\sim 50\,\%$ and $\sim 40\,\%$ (Fig. 3a), which is a well-known ERH range of pure AS (Winston and Bates, 1960). At $\sim 50\,\%$ RH, a population of effloresced particles and non-effloresced particles coexisted on the substrate, and when the needle poked the AS–H_2O particles, all particles including non-effloresced particles cracked (Fig. 1b). The act of poking non-effloresced particles at a RH close to that ERH of AS may induce the nucleation of an AS crystal, similar to the well-known process of contact freezing of supercooled cloud droplets (e.g., Ciobanu et al., 2010; Ladino et al., 2011; Hoose and Möhler, 2012). All particles, regardless of whether already effloresced or not, cracked when poked at a RH $\leq \sim 50\,\%$. Moreover, when we tried to poke the particles

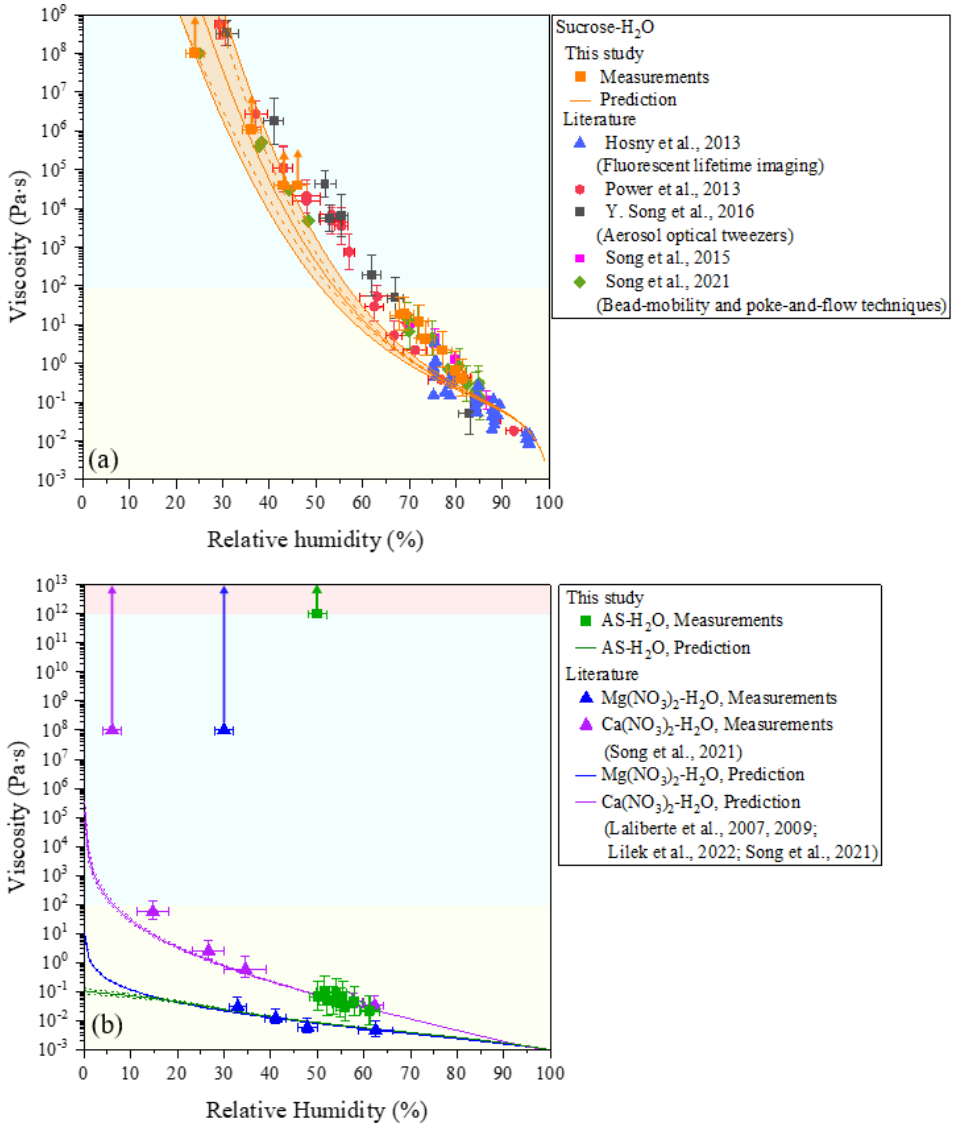

Figure 2. Viscosities of measurements for AIOMFAC-VISC predictions of binary systems consisting of **(a)** sucrose–H_2O and **(b)** ammonium sulfate (AS)–H_2O at 293 ± 1 K. Mean viscosities are results from bead-mobility experiments with the error of x axis representing standardization of three to five beads in one or two particles at given relative humidity (RH). The upper limit and lower limit of the y axis are produced by 95 % prediction bands of the calibration curve for the ratio of bead speed to viscosity (Fig. S1). Arrows indicate lower limits to viscosity obtained from poke-and-flow experiments (Sect. S2) determined from experimental flow time (Fig. S4) and the equation by Sellier et al. (2015). When particles containing sucrose cracked due to poking, a lower limit of the viscosity of the particle is determined to be $\sim 1 \times 10^8$ Pa s. The light yellow region is the liquid phase, the light blue region is the semisolid phase, and the light red region is the solid phase. The viscosity of sucrose–H_2O particles agrees with the results of previous studies included in **(a)**. Previous studies on viscosities of measurement and AIOMFAC-VISC predictions for binary systems of $Mg(NO_3)_2$–H_2O, and $Ca(NO_3)_2$–H_2O from Song et al. (2021) are also included in **(b)**. AIOMFAC-VISC predictions with the Zdanovskii–Stokes–Robinson (ZSR) organic–inorganic mixing model for viscosity. Model sensitivity, defined by the impact of ± 2 % variation in aerosol water content, is shown by the dashed curves. The orange shaded region in **(a)** shows the potential viscosity prediction error introduced by ± 5 % error in the glass transition temperature of sucrose.

at ~ 55 % RH, the $\tau_{(exp,\,flow)}$ of the particles was fast, corresponding to a liquid-like physical state and flow behavior. Based on the observed contrasting behavior at lower RH, the AS–H_2O particles were determined to be in a solid state for RH $\leq \sim 50$ %.

3.2 Viscosities in ternary systems of sucrose–AS–H_2O with different mixing ratios

To mimic atmospherically relevant aerosol particles containing both organics, water and inorganic ions, we mixed sucrose and AS. Moreover, to explore how viscosity varies de-

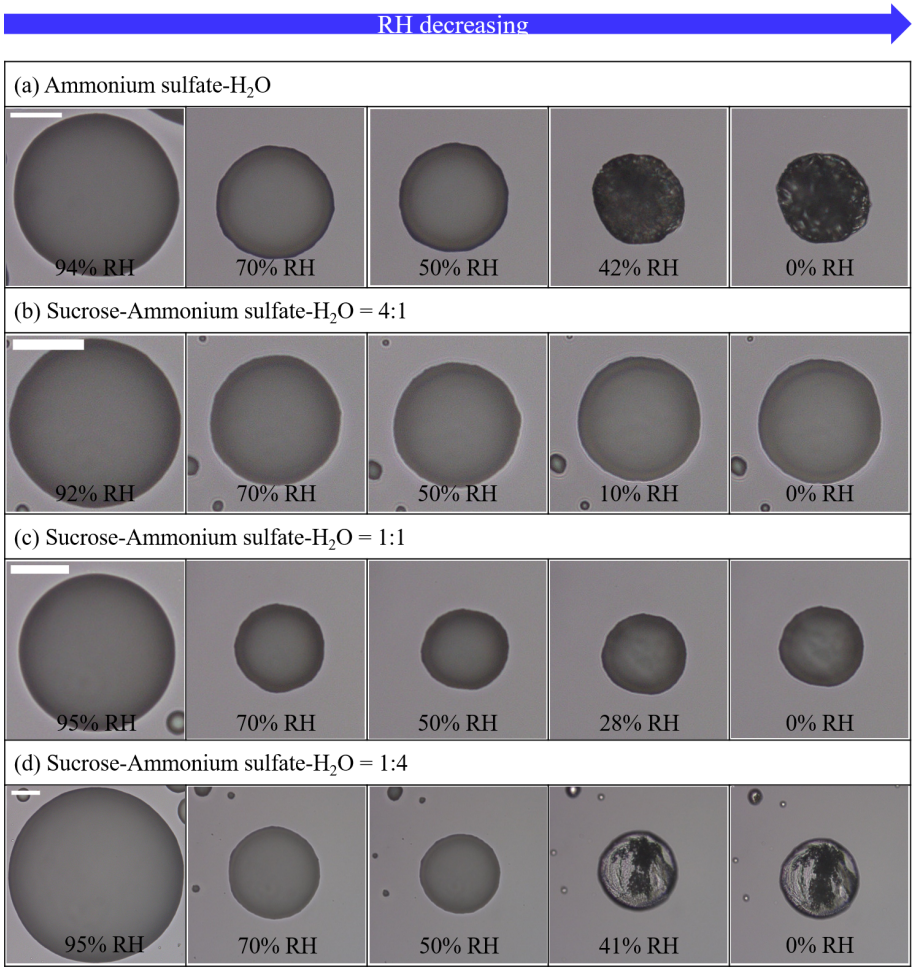

Figure 3. Optical images on dehydration process at a temperature of 290 ± 1 K for **(a)** ammonium sulfate (AS)–H_2O, **(b)** sucrose–AS–H_2O for organic-to-inorganic dry ratios (OIRs) = 4 : 1, **(c)** sucrose–AS–H_2O particles for OIR = 1 : 1 and **(d)** sucrose–AS–H_2O particles for OIR = 1 : 4 at a rate of dehydration of 0.3 % RH min^{-1}–0.5 % RH min^{-1}. White scale bar indicates 20 µm.

pending on the mixing ratio of sucrose–AS–H_2O particles, we investigated three different OIRs of 4 : 1, 1 : 1, and 1 : 4.

For organic-rich particles of sucrose–AS–H_2O (OIR = 4 : 1), the mean viscosity was quantified from the bead-mobility technique as $\sim 1 \times 10^{-1}$ to $\sim 5 \times 10^{1}$ Pa s as RH decreased from ~ 81 % to ~ 53 % (blue symbols in Fig. 4). From the poke-and-flow technique, the lower limit to the viscosities was determined to be $\sim 4 \times 10^{3}$ Pa s for ~ 35 % RH, $\sim 8 \times 10^{4}$ Pa s for ~ 30 % RH, and $\sim 1 \times 10^{5}$ Pa s for ~ 28 % (Fig. 4). At RH of ~ 25 %, it was difficult to determine the viscosity using the poke-and-flow technique because the inner hole formed on poking did not close even during 24 h. The particles clearly cracked at ~ 18 % RH as shown in Fig. 1c, and this produces the lower limit to the viscosity of $\sim 1 \times 10^{8}$ Pa s (Renbaum-Wolff et al., 2013a; Grayson et al., 2015; Song et al., 2019; Song et al., 2021). A gradual increase in the viscosities was observed in the particles of sucrose–AS–H_2O for an OIR of 4 : 1, as RH decreased (Fig. 4). Such a gradual increase in viscosity of the organic-rich particles is similar to that of sucrose–H_2O particles (Fig. 2a), but the viscosity values of the sucrose–AS–H_2O particles at this OIR are approximately 2 orders of magnitude lower than those of sucrose–H_2O particles at the same RH. In addition, the finding of gradual enhancements in the organic-rich particle is inconsistent with the result of other recent viscosity studies of SOA particles (Song et al., 2015; Grayson et al., 2016; Hosny et al., 2016; M. Song et al., 2016; Song et al., 2019; Gervasi et al., 2020; Maclean et al., 2021; Smith et al., 2021). The viscosities of the sucrose–AS–H_2O for OIR = 4 : 1 correspond to liquid for RH > ~ 53 %, semisolid for ~ 18 % < RH < ~ 50 %, and semisolid or solid for RH < ~ 18 %. It is interesting to note that any likely crystallization and/or efflorescence process of AS in the organic-rich particle was not observable in the optical images on the dehydration process down to ~ 0 % RH (Fig. 3b). Previous studies have shown such behavior that organic-rich or SOA particles also cracked upon poking, without the appearance of crystallization (Song et al., 2019, 2021; Smith et al., 2021).

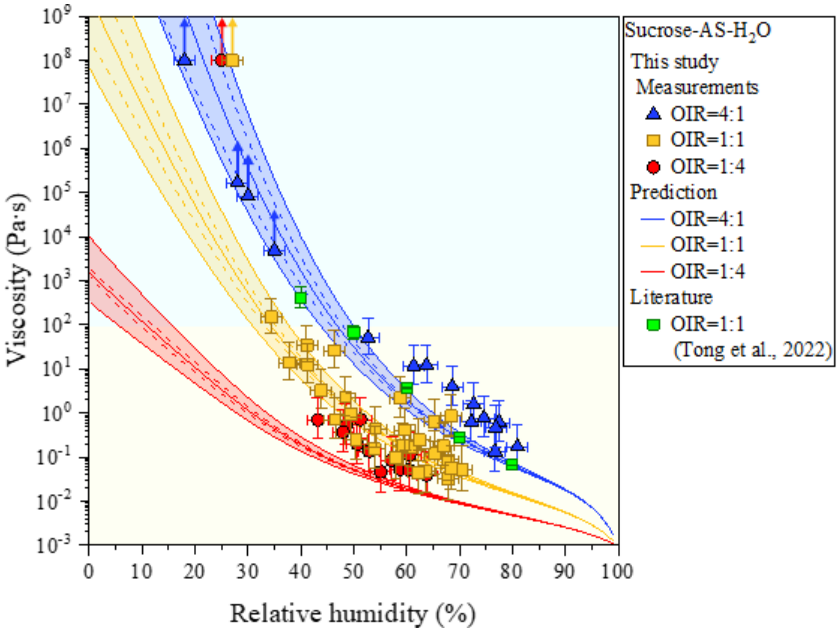

Figure 4. Viscosities as a function of relative humidity (RH), with measurements from bead-mobility and poke-and-flow experiments and AIOMFAC-VISC predictions of ternary systems of sucrose–ammonium sulfate (AS)–H_2O particles for organic-to-inorganic dry ratios (OIRs) = 4 : 1, 1 : 1, and 1 : 4 at 293 ± 1 K. Arrows indicate lower limits to viscosity obtained from poke-and-flow experiments (Sect. S2) determined from the experimental flow time (Fig. S4) and equation reported from Sellier et al. (2015). When particles containing sucrose cracked by poking, the estimated lower limit of the viscosity of a particle was $\sim 1 \times 10^8$ Pa s. Mean viscosities are the result of bead-mobility experiments with the error along the x-axis direction representing standardization of three to five beads in one or two particles at given RH. The upper limit and lower limit along the y axis are produced by 95 % prediction bands of the calibration curve for the ratio of bead speed to viscosity (Fig. S1). The light yellow region is the liquid phase, and the light blue region is the semisolid phase. Viscosity of sucrose–AS–H_2O particles for OIR = 1 : 1 using an aerosol optical tweezers system at 297 K is also included (Tong et al., 2022). AIOMFAC-VISC predictions with the Zdanovskii–Stokes–Robinson (ZSR) organic–inorganic mixing model for viscosity. Model sensitivity, defined by the impact of ± 2 % variation in aerosol water content, is shown by the dashed curves. Shaded regions show the potential viscosity prediction error introduced by ± 5 % error in the glass transition temperature of sucrose. See Fig. S5 for comparison to AIOMFAC-VISC predictions using the aquelec mixing model.

In particles consisting of sucrose–AS–H_2O particles with an OIR = 1 : 1, the mean viscosity varied from $\sim 5 \times 10^{-2}$ to $\sim 1 \times 10^2$ Pa s from ∼ 70 % to ∼ 34 % RH (yellow symbols in Fig. 4). At ∼ 30 % RH, we could not determine the viscosity using the poke-and-flow technique because the droplets were supersaturated with respect to AS upon dehydration. The particles cracked by poking at ∼ 27 % RH (Fig. 1d), so the lower limit of the viscosity of the particle was estimated as $\sim 1 \times 10^8$ Pa s (Fig. 4). At the close RH where particles cracked, the particles crystallized or effloresced, although it was not accurately observed optically (Fig. 3c). The viscosities of sucrose–AS–H_2O particles for an OIR = 1 : 1 using an optical tweezers are also included in Fig. 4 (Tong et al., 2022). Results showed that viscosities for sucrose–AS droplets from this study and Tong et al. (2022) are consistent within ∼ 1 order of magnitude at given RH. The viscosity deviations at given RH when comparing the two series of measurements may come from uncertainties associated with the different techniques, temperature ranges, and mode of RH changes (i.e., decreasing or increasing RH). From the RH-dependent viscosities, our result showed that sucrose–AS–H_2O particles with an OIR = 1 : 1 existed as liquid for RH > ∼ 34 %, semisolid for ∼ 34 % < RH < ∼ 27 %, and semisolid or solid for RH < ∼ 27 % (Fig. 4).

For inorganic-rich particles of sucrose–AS–H_2O (OIR = 1 : 4), the mean viscosity ranged from $\sim 4 \times 10^{-2}$ to $\sim 7 \times 10^{-1}$ Pa s for an RH range of ∼ 64 % to ∼ 43 % determined from the bead-mobility technique (red symbols in Fig. 4). This viscosity result of sucrose–AS–H_2O for OIR = 1 : 4 observed in the RH range (Fig. 4) is similar to the result in the binary system of AS–H_2O free of organic particles at the same RH within experimental errors (Fig. 2b). In the RH range from ∼ 40 % to ∼ 30 % we could not quantify the viscosities of the particles with sufficient accuracy, neither with the bead-mobility nor the poke-and-flow techniques. In this RH range, the bead movements inside the particles were too slow to observe and quantify. In addition, when we poked the particles, the particles would stick to the needle, rendering that approach unsuitable. Upon dehydration, the particles crystallized or effloresced

at $\sim 40 \pm 2.0$ % RH (Fig. 3d), which is close to the ERH of an organic-free AS droplet (Winston and Bates, 1960). At the RH, the particle was observed containing a multiphase nature from the optical image (Fig. 3d). While the presence of a crystalline AS phase is likely (compare Fig. 3a and d), it is unclear whether the remaining liquid forms a more structured gel state or an amorphous viscous semisolid or solid state. This ternary system may therefore be of interest for future studies employing other probing techniques and phase composition analysis. At lower RH of ~ 25 %, the inorganic-rich sucrose–AS–H_2O particles shattered without any flow of the material for 3 h (Fig. 1e), corresponding to the lower limit of the viscosity of $\sim 1 \times 10^8$ Pa s. These results lead to a drastic enhancement in viscosity of approximately 8 orders of magnitude in RH from 43 % to 25 % of the particles as illustrated in Fig. 4 (red symbols), which is comparable to the gradual enhancement in viscosity of the organic-rich particles (blue symbols). Also, recent studies of Richards et al. (2020b) and Song et al. (2021) showed such a drastic increase in viscosities when inorganic species of $CaCl_2$, $MgSO_4$, $Ca(NO_3)_2$, or $Mg(NO_3)_2$ were mixed with organic compounds (e.g., glucose or sucrose). Based on the viscosity values, particles with an OIR of 1 : 4 were in a liquid state for RH $> \sim 43$ %, in a semisolid state for ~ 25 % < RH < ~ 43 %, and in a semisolid or solid state for RH < ~ 25 %.

3.3 Comparison of viscosity predictions and measurements

AIOMFAC-VISC predictions for binary sucrose–H_2O, $Ca(NO_3)_2$–H_2O, $Mg(NO_3)_2$–H_2O, and AS–H_2O are shown in Fig. 2. The predicted viscosity for binary sucrose–H_2O agrees well within the error of the measurements, but it does not capture the full spread of measurements for RH between 65 % and 85 %. The binary $Ca(NO_3)_2$–H_2O, $Mg(NO_3)_2$–H_2O, and AS–H_2O predictions agree well within the error of the measurements for RH < ~ 25 % (and excluding the measurements at 10^8 Pa s that indicate crystallization). Also, the predicted viscosity for $Ca(NO_3)_2$–H_2O is less than the measured viscosity at RH = ~ 15 %. Unlike the predicted viscosities for $Ca(NO_3)_2$–H_2O and $Mg(NO_3)_2$–H_2O, the AS–H_2O prediction curve does not undergo a steep increase for RH < ~ 10 %, due to the weaker influence of cation–anion pairs for this system compared to systems containing a divalent cation (e.g., Ca^{2+} or Mg^{2+}). We also note that the AIOMFAC-VISC calculations were carried out for single liquid phases of these salt solutions, in which crystallization is suppressed, providing an estimate of the liquid-state viscosity for conditions where the salt would crystallize in an experiment.

Shown in Fig. 4 are the measurement and model comparisons of the RH-dependent viscosities of the sucrose–AS–H_2O systems with OIRs of 4 : 1, 1 : 1, and 1 : 4. The model predictions and measurements agree well for all three OIRs, with the model predicting viscosities mostly within the error of the measurements. For the system studied in this work, the predictions using the ZSR mixing approach for viscosity (Fig. 4) are consistently better than those using the aquelec mixing approach (Fig. S5 in the Supplement). The ZSR mixing approach likely performs better than aquelec because it puts more weight on the binary aqueous sucrose contribution to the predicted mixed-phase viscosity. By contrast, aquelec puts more weight on the viscosity contribution from the aqueous electrolyte solution (i.e., AS–H_2O), driving the organic–inorganic mixture viscosity lower. This is especially noticeable for the OIR = 1 : 4 curve in Fig. S5 when compared to that in Fig. 4.

The most significant deviations between the model and the measurements are for OIR = 1 : 1 and OIR = 1 : 4 at RH below 30 %, and these are expected based on similar findings in the study by Song et al. (2021). When particles cracked during poke-and-flow experiments, perhaps due to crystallization of the solutes, the lower limit of viscosity was reported as $\sim 10^8$ Pa s. In these calculations with AIOMFAC-VISC, the predictions do not account for phase changes such as crystallization (or a gel transition), which explains why the model does not reproduce the measurements at these points. However, the model provides an estimate for the viscosity of the particle phase had AS not crystallized. For the organic-rich case (OIR = 4 : 1), it is expected that the relative abundance of sucrose impedes or completely inhibits crystallization, such that a smooth increase in viscosity is observed instead, with very good model–measurement agreement.

4 Summary

In this study, the viscosities of particles in binary systems of sucrose–H_2O and AS–H_2O and ternary systems of sucrose–AS–H_2O for OIRs of 4 : 1, 1 : 1, and 1 : 4 for decreasing RH were quantified by bead-mobility and poke-and-flow techniques at 293 ± 1 K. Viscosity of sucrose–H_2O particles increased gradually from $\sim 4 \times 10^{-1}$ to $> \sim 1 \times 10^8$ Pa s when the RH decreased from ~ 81 % to ~ 24 % while the viscosity of AS–H_2O particles increased drastically to $\sim 10^{12}$ Pa s at ~ 50 % RH. For the ternary systems, the viscosity of organic-rich (OIR = 4 : 1) particles gradually increased from $\sim 1 \times 10^{-1}$ to $\sim 1 \times 10^8$ Pa s with a reduction of RH from ~ 81 % to ~ 18 %, showing a tendency similar to that of the sucrose–H_2O particle; however, viscosities observed were ~ 2 orders of magnitude lower in the sucrose–AS–H_2O particles. Particles consisting of sucrose–AS–H_2O with an OIR of 1 : 1 ranged in viscosity from $\sim 5 \times 10^{-2}$ to $\sim 1 \times 10^8$ Pa s for an RH range of ~ 70 to ~ 27 %. When the fraction of the inorganic salt was higher (OIR = 1 : 4), sharp enhancement of viscosity was indicated with values of $\sim 4 \times 10^{-2}$ to $\sim 1 \times 10^8$ Pa s for RH ranging from ~ 64 % to ~ 25 % as in the case of AS–H_2O particles. Based on the viscosity results, the particles of binary and ternary systems ranged from liquid

to semisolid, and even the solid state depending on the RH. Moreover, the values of measured viscosities of sucrose–AS–H_2O particles were compared to the values of AIOMFAC-VISC predicted viscosities of sucrose–AS–H_2O particles for OIRs of 4 : 1, 1 : 1, and 1 : 4. The model–measurement comparison showed very good agreement considering the uncertainties and sensitivity estimates of the measurements and the model, at least for the RH range in which crystallization of the salt could be ruled out. Comparison of the predictions for the three OIRs also suggests that the ZSR-based viscosity prediction approach for organic–inorganic mixtures is superior to that of the "aquelec" method for the sucrose–AS–H_2O system.

Data availability. Underlying material and related data for this paper are provided in the Supplement.

Supplement. The supplement related to this article is available online at: https://doi.org/10.5194/acp-22-8805-2022-supplement.

Author contributions. MS designed this study. RJ and MS conducted viscosity experiments and analyzed the data. JL and AZ conducted AIOMFAC-VISC model predictions and wrote the related sections. RJ and MS prepared the article with contributions from JL, AZ, RX, MNC, DK, and HM.

Competing interests. The contact author has declared that none of the authors has any competing interests.

Disclaimer. Publisher's note: Copernicus Publications remains neutral with regard to jurisdictional claims in published maps and institutional affiliations.

Acknowledgements. Mijung Song gives thanks to Hyeok Jin Kim for the technical support.

Financial support. This work was supported by the National Research Foundation of Korea (NRF) grant funded by the South Korean government (MSIT) (NRF-2019R1A2C1086187), by the Fine Particle Research Initiative in East Asia Considering National Differences (FRIEND) project (NRF-2020M3G1A1114548), and by the Technology Development Program to Solve Climate Changes of the National Research Foundation (NRF) funded by the South Korean government (MSIT) (NRF-2019M1A2A2103956). This project was undertaken with the financial support of the government of Canada through the federal Department of Environment and Climate Change (grant no. GCXE20S049). This work was also supported by the Alfred P. Sloan Foundation under Prime Award no. G-2020-13912.

Review statement. This paper was edited by Daniel Knopf and reviewed by two anonymous referees.

References

Athanasiadis, A., Fitzgerald, C., Davidson, N. M., Giorio, C., Botchway, S. W., Ward, A. D., Kalberer, M., Pope, F. D., and Kuimova, M. K.: Dynamic viscosity mapping of the oxidation of squalene aerosol particles, Phys. Chem. Chem. Phys., 18, 30385–30393, https://doi.org/10.1039/C6CP05674A, 2016.

Bateman, A. P., Bertram, A. K., and Martin, S. T.: Hygroscopic influence on the semisolid-to-liquid transition of secondary organic materials, J. Phys. Chem. A, 119, 4386–4395, https://doi.org/10.1021/jp508521c, 2015.

Bateman, A. P., Gong, Z., Harder, T. H., de Sá, S. S., Wang, B., Castillo, P., China, S., Liu, Y., O'Brien, R. E., Palm, B. B., Shiu, H.-W., Cirino, G. G., Thalman, R., Adachi, K., Alexander, M. L., Artaxo, P., Bertram, A. K., Buseck, P. R., Gilles, M. K., Jimenez, J. L., Laskin, A., Manzi, A. O., Sedlacek, A., Souza, R. A. F., Wang, J., Zaveri, R., and Martin, S. T.: Anthropogenic influences on the physical state of submicron particulate matter over a tropical forest, Atmos. Chem. Phys., 17, 1759–1773, https://doi.org/10.5194/acp-17-1759-2017, 2017.

Berkemeier, T., Steimer, S. S., Krieger, U. K., Peter, T., Pöschl, U., Ammann, M., and Shiraiwa, M.: Ozone uptake on glassy, semi-solid and liquid organic matter and the role of reactive oxygen intermediates in atmospheric aerosol chemistry, Phys. Chem. Chem. Phys., 18, 12662–12674, https://doi.org/10.1039/C6CP00634E, 2016.

Bertram, A. K., Martin, S. T., Hanna, S. J., Smith, M. L., Bodsworth, A., Chen, Q., Kuwata, M., Liu, A., You, Y., and Zorn, S. R.: Predicting the relative humidities of liquid-liquid phase separation, efflorescence, and deliquescence of mixed particles of ammonium sulfate, organic material, and water using the organic-to-sulfate mass ratio of the particle and the oxygen-to-carbon elemental ratio of the organic component, Atmos. Chem. Phys., 11, 10995–11006, https://doi.org/10.5194/acp-11-10995-2011, 2011.

Bhattarai, G., Lee, J. B., Kim, M.-H., Ham, S., So, H.-S., Oh, S., Sim, H.-J., Lee, J.-C., Song, M., and Kook, S.-H.: Maternal exposure to fine particulate matter during pregnancy induces progressive senescence of hematopoietic stem cells under preferential impairment of the bone marrow microenvironment and aids development of myeloproliferative disease, Leukemia, 34, 1481–1484, https://doi.org/10.1038/s41375-019-0665-8, 2020.

Bouzidi, H., Zuend, A., Ondráček, J., Schwarz, J., and Ždímal, V.: Hygroscopic behavior of inorganic–organic aerosol systems including ammonium sulfate, dicarboxylic acids, and oligomer, Atmos. Environ., 229, 117481, https://doi.org/10.1016/j.atmosenv.2020.117481, 2020.

Braban, C. F. and Abbatt, J. P. D.: A study of the phase transition behavior of internally mixed ammonium sulfate - malonic acid aerosols, Atmos. Chem. Phys., 4, 1451–1459, https://doi.org/10.5194/acp-4-1451-2004, 2004.

Ciobanu, V. G., Marcolli, C., Krieger, U. K., Weers, U., and Peter, T.: Liquid-liquid phase separation in mixed organic/inorganic aerosol particles, J. Phys. Chem. A, 113, 10966–10978, https://doi.org/10.1021/jp905054d, 2009.

Ciobanu, V. G., Marcolli, C., Krieger, U. K., Zuend, A., and Peter, T.: Efflorescence of ammonium sulfate and coated ammonium sulfate particles: Evidence for surface nucleation, Phys. Chem. A, 114, 9486–9495, https://doi.org/10.1021/jp103541w, 2010.

Davies, J. F. and Wilson, K. R.: Nanoscale interfacial gradients formed by the reactive uptake of OH radicals onto viscous aerosol surfaces, Chem. Sci., 6, 7020–7027, https://doi.org/10.1039/C5SC02326B, 2015.

Dehaoui, A., Issenmann, B., and Caupin, F.: Viscosity of deeply supercooled water and its coupling to molecular diffusion, P. Natl. Acad. Sci. USA, 112, 12020–12025, https://doi.org/10.1073/pnas.1508996112, 2015.

DeRieux, W.-S. W., Li, Y., Lin, P., Laskin, J., Laskin, A., Bertram, A. K., Nizkorodov, S. A., and Shiraiwa, M.: Predicting the glass transition temperature and viscosity of secondary organic material using molecular composition, Atmos. Chem. Phys., 18, 6331–6351, https://doi.org/10.5194/acp-18-6331-2018, 2018.

Glasstone, S., Laidler, K. J., and Eyring, H.: The theory of rate processes; the kinetics of chemical reactions, viscosity, diffusion and electrochemical phenomena, McGraw-Hill, 1st Edn., ISBN 13 9780070233607, 1941.

Gervasi, N. R., Topping, D. O., and Zuend, A.: A predictive group-contribution model for the viscosity of aqueous organic aerosol, Atmos. Chem. Phys., 20, 2987–3008, https://doi.org/10.5194/acp-20-2987-2020, 2020.

Grayson, J. W., Song, M., Sellier, M., and Bertram, A. K.: Validation of the poke-flow technique combined with simulations of fluid flow for determining viscosities in samples with small volumes and high viscosities, Atmos. Meas. Tech., 8, 2463–2472, https://doi.org/10.5194/amt-8-2463-2015, 2015.

Grayson, J. W., Zhang, Y., Mutzel, A., Renbaum-Wolff, L., Böge, O., Kamal, S., Herrmann, H., Martin, S. T., and Bertram, A. K.: Effect of varying experimental conditions on the viscosity of α-pinene derived secondary organic material, Atmos. Chem. Phys., 16, 6027–6040, https://doi.org/10.5194/acp-16-6027-2016, 2016.

Ham, S., Babar, Z. B., Lee, J. B., Lim, H.-J., and Song, M.: Liquid–liquid phase separation in secondary organic aerosol particles produced from α-pinene ozonolysis and α-pinene photooxidation with/without ammonia, Atmos. Chem. Phys., 19, 9321–9331, https://doi.org/10.5194/acp-19-9321-2019, 2019.

Hodas, N., Zuend, A., Mui, W., Flagan, R. C., and Seinfeld, J. H.: Influence of particle-phase state on the hygroscopic behavior of mixed organic–inorganic aerosols, Atmos. Chem. Phys., 15, 5027–5045, https://doi.org/10.5194/acp-15-5027-2015, 2015.

Hoose, C. and Möhler, O.: Heterogeneous ice nucleation on atmospheric aerosols: a review of results from laboratory experiments, Atmos. Chem. Phys., 12, 9817–9854, https://doi.org/10.5194/acp-12-9817-2012, 2012.

Hosny, N. A., Fitzgerald, C., Tong, C., Kalberer, M., Kuimova, M. K., and Pope, F. D.: Fluorescent lifetime imaging of atmospheric aerosols: a direct probe of aerosol viscosity, Faraday Discuss., 165, 343–356, https://doi.org/10.1039/C3FD00041A, 2013.

Hosny, N. A., Fitzgerald, C., Vyšniauskas, A., Athanasiadis, A., Berkemeier, T., Uygur, N., Pöschl, U., Shiraiwa, M., Kalberer, M., Pope, F. D., and Kuimova, M. K.: Direct imaging of changes in aerosol particle viscosity upon hydration and chemical aging, Chem. Sci., 7, 1357–1367, https://doi.org/10.1039/C5SC02959G, 2016.

IPCC: IPCC Special Report on the Ocean and Cryosphere in a Changing Climate, edited by: Pörtner, H.-O., Roberts, D. C., Masson-Delmotte, V., Zhai, P., Tignor, M., Poloczanska, E., Mintenbeck, K., Alegría, A, Nicolai, M., Okem, A., Petzold, J., and Rama, B., Weyer, N. M., 755 pp., https://doi.org/10.1017/9781009157964, 2019.

Jimenez, J. L., Canagaratna, M. R., Donahue, N. M., Prevot, A. S., Zhang, Q., Kroll, J. H., DeCarlo, P. F., Allan, J. D., Coe, H., Ng, N. L., Aiken, A. C., Docherty, K. S., Ulbrich, I. M., Grieshop, A. P., Robinson, A. L., Duplissy, J., Smith, J. D., Wilson, K. R., Lanz, V. A., Hueglin, C., Sun, Y. L., Tian, J., Laaksonen, A., Raatikainen, T., Rautiainen, J., Vaattovaara, P., Ehn, M., Kulmala, M., Tomlinson, J. M., Collins, D. R., Cubison, M. J., Dunlea, E. J., Huffman, J. A., Onasch, T. B., Alfarra, M. R., Williams, P. I., Bower, K., Kondo, Y., Schneider, J., Drewnick, F., Borrmann, S., Weimer, S., Demerjian, K., Salcedo, D., Cottrell, L., Griffin, R., Takami, A., Miyoshi, T., Hatakeyama, S., Shimono, A., Sun, J. Y., Zhang, Y. M., Dzepina, K., Kimmel, J. R., Sueper, D., Jayne, J. T., Herndon, S. C., Trimborn, A. M., Williams, L. R., Wood, E. C., Middlebrook, A. M., Kolb, C. E., Baltensperger, U., and Worsnop, D. R.: Evolution of organic aerosols in the atmosphere, Science, 326, 1525–1529, https://doi.org/10.1126/science.1180353, 2009.

Knopf, D. A.: Thermodynamic properties and nucleation processes of upper tropospheric and lower stratospheric aerosol particles, ETH Zurich, Diss. ETH No. 15103, Zurich, Switzerland, 2003.

Koop, T., Bookhold, J., Shiraiwa, M., and Pöschl, U.: Glass transition and phase state of organic compounds: dependency on molecular properties and implications for secondary organic aerosols in the atmosphere, Phys. Chem. Chem. Phys., 13, 19238–19255, https://doi.org/10.1039/C1CP22617G, 2011.

Kulmala, M., Arola, A., Nieminen, T., Riuttanen, L., Sogacheva, L., de Leeuw, G., Kerminen, V.-M., and Lehtinen, K. E. J.: The first estimates of global nucleation mode aerosol concentrations based on satellite measurements, Atmos. Chem. Phys., 11, 10791–10801, https://doi.org/10.5194/acp-11-10791-2011, 2011.

Kuwata, M. and Martin, S. T.: Phase of atmospheric secondary organic material affects its reactivity, P. Natl. Acad. Sci. USA, 109, 17354–17359, 2012.

Ladino, L., Stetzer, O., Lüönd, F., Welti, A., and Lohmann, U.: Contact freezing experiments of kaolinite particles with cloud droplets, J. Geophys. Res.-Atmos., 116, D22202, https://doi.org/10.1029/2011JD015727, 2011.

Laliberté, M.: Model for calculating the viscosity of aqueous aolutions, J. Chem. Eng. Data, 52, 1507–1508, https://doi.org/10.1021/je700232s, 2007.

Laliberté, M.: A model for calculating the heat capacity of aqueous solutions, with updated density and viscosity data, J. Chem. Eng. Data, 54, 1725–1760, https://doi.org/10.1021/je8008123, 2009.

Lam, H. K., Xu, R., Choczynski, J., Davies, J. F., Ham, D., Song, M., Zuend, A., Li, W., Tse, Y.-L. S., and Chan, M. N.: Effects of liquid–liquid phase separation and relative humidity on the heterogeneous OH oxidation of inorganic–organic aerosols: insights from methylglutaric acid and ammonium sulfate particles, Atmos. Chem. Phys., 21, 2053–2066, https://doi.org/10.5194/acp-21-2053-2021, 2021.

Li, J., Forrester, S. M., and Knopf, D. A.: Heterogeneous oxidation of amorphous organic aerosol surrogates by O_3, NO_3, and OH

at typical tropospheric temperatures, Atmos. Chem. Phys., 20, 6055–6080, https://doi.org/10.5194/acp-20-6055-2020, 2020.

Lilek, J. and Zuend, A.: A predictive viscosity model for aqueous electrolytes and mixed organic–inorganic aerosol phases, Atmos. Chem. Phys., 22, 3203–3233, https://doi.org/10.5194/acp-22-3203-2022, 2022.

Liu, D., Joshi, R., Wang, J., Yu, C., Allan, J. D., Coe, H., Flynn, M. J., Xie, C., Lee, J., Squires, F., Kotthaus, S., Grimmond, S., Ge, X., Sun, Y., and Fu, P.: Contrasting physical properties of black carbon in urban Beijing between winter and summer, Atmos. Chem. Phys., 19, 6749–6769, https://doi.org/10.5194/acp-19-6749-2019, 2019.

Maclean, A. M., Smith, N. R., Li, Y., Huang, Y., Hettiyadura, A. P., Crescenzo, G. V., Shiraiwa, M., Laskin, A., Nizkorodov, S. A., and Bertram, A. K.: Humidity-Dependent Viscosity of Secondary Organic Aerosol from Ozonolysis of β-Caryophyllene: Measurements, Predictions, and Implications, ACS Earth Space Chem., 5, 305–318, https://doi.org/10.1021/acsearthspacechem.0c00296, 2021.

Marcolli, C.: Deposition nucleation viewed as homogeneous or immersion freezing in pores and cavities, Atmos. Chem. Phys., 14, 2071–2104, https://doi.org/10.5194/acp-14-2071-2014, 2014.

Martin, S. T.: Phase transitions of aqueous atmospheric particles, Chem. Rev., 100, 3403–3454, https://doi.org/10.1021/cr990034t, 2000.

Murphy, D., Cziczo, D., Froyd, K., Hudson, P., Matthew, B., Middlebrook, A., Peltier, R., Sullivan, A., Thomson, D., and Weber, R.: Single-particle mass spectrometry of tropospheric aerosol particles, J. Geophys. Res.-Atmos., 111, D23S32, https://doi.org/10.1029/2006JD007340, 2006.

Murray, B. J., Haddrell, A. E., Peppe, S., Davies, J. F., Reid, J. P., O'Sullivan, D., Price, H. C., Kumar, R., Saunders, R. W., Plane, J. M. C., Umo, N. S., and Wilson, T. W.: Glass formation and unusual hygroscopic growth of iodic acid solution droplets with relevance for iodine mediated particle formation in the marine boundary layer, Atmos. Chem. Phys., 12, 8575–8587, https://doi.org/10.5194/acp-12-8575-2012, 2012.

O'Brien, R. E., Neu, A., Epstein, S. A., MacMillan, A. C., Wang, B., Kelly, S. T., Nizkorodov, S. A., Laskin, A., Moffet, R. C., and Gilles, M. K.: Physical properties of ambient and laboratory-generated secondary organic aerosol, Geophys. Res. Lett., 41, 4347–4353, 2014.

Pant, A., Parsons, M. T., and Bertram, A. K.: Crystallization of aqueous ammonium sulfate particles internally mixed with soot and kaolinite: Crystallization relative humidities and nucleation rates, Phys. Chem. A, 110, 8701–8709, https://doi.org/10.1021/jp060985s, 2006.

Perraud, V., Bruns, E. A., Ezell, M. J., Johnson, S. N., Yu, Y., Alexander, M. L., Zelenyuk, A., Imre, D., Chang, W. L., and Dabdub, D.: Nonequilibrium atmospheric secondary organic aerosol formation and growth, P. Natl. Acad. Sci. USA, 109, 2836–2841, https://doi.org/10.1073/pnas.1119909109, 2012.

Petters, S. S., Kreidenweis, S. M., Grieshop, A. P., Ziemann, P. J., and Petters, M. D.: Temperature-and humidity-dependent phase states of secondary organic aerosols, Geophys. Res. Lett., 46, 1005–1013, https://doi.org/10.1029/2018GL080563, 2019.

Power, R., Simpson, S., Reid, J., and Hudson, A.: The transition from liquid to solid-like behaviour in ultra-high viscosity aerosol particles, Chem. Sci., 4, 2597–2604, https://doi.org/10.1039/C3SC50682G, 2013.

Renbaum-Wolff, L., Grayson, J. W., and Bertram, A. K.: Technical Note: New methodology for measuring viscosities in small volumes characteristic of environmental chamber particle samples, Atmos. Chem. Phys., 13, 791–802, https://doi.org/10.5194/acp-13-791-2013, 2013a.

Renbaum-Wolff, L., Grayson, J. W., Bateman, A. P., Kuwata, M., Sellier, M., Murray, B. J., Shilling, J. E., Martin, S. T., and Bertram, A. K.: Viscosity of α-pinene secondary organic material and implications for particle growth and reactivity, P. Natl. Acad. Sci. USA, 110, 8014–8019, https://doi.org/10.1073/pnas.1219548110, 2013b.

Richards, D. S., Trobaugh, K. L., Hajek-Herrera, J., and Davis, R. D.: Dual-Balance Electrodynamic Trap as a Microanalytical Tool for Identifying Gel Transitions and Viscous Properties of Levitated Aerosol Particles, Anal. Chem., 92, 3086–3094, https://doi.org/10.1021/acs.analchem.9b04487, 2020a.

Richards, D. S., Trobaugh, K. L., Hajek-Herrera, J., Price, C. L., Sheldon, C. S., Davies, J. F., and Davis, R. D.: Ion-molecule interactions enable unexpected phase transitions in organic-inorganic aerosol, Sci. Adv., 6, eabb5643, 2020b.

Rovelli, G., Song, Y.-C., Maclean, A. M., Topping, D. O., Bertram, A. K., and Reid, J. P.: Comparison of approaches for measuring and predicting the viscosity of ternary component aerosol particles, Anal. Chem., 91, 5074–5082, https://doi.org/10.1021/acs.analchem.8b05353, 2019.

Sellier, M., Grayson, J., Renbaum-Wolff, L., Song, M., and Bertram, A.: Estimating the viscosity of a highly viscous liquid droplet through the relaxation time of a dry spot, Rheology, 59, 733–750, https://doi.org/10.1122/1.4917240, 2015.

Slade, J. H. and Knopf, D. A.: Multiphase OH oxidation kinetics of organic aerosol: The role of particle phase state and relative humidity, Geophys. Res. Lett., 41, 5297–5306, https://doi.org/10.1002/2014GL060582, 2014.

Smith, N. R., Crescenzo, G. V., Huang, Y., Hettiyadura, A. P., Siemens, K., Li, Y., Faiola, C. L., Laskin, A., Shiraiwa, M., and Bertram, A. K.: Viscosity and liquid–liquid phase separation in healthy and stressed plant SOA, Environmental Science Atmospheres, 1, 140–153, https://doi.org/10.1039/D0EA00020E, 2021.

Song, M., Liu, P. F., Hanna, S. J., Li, Y. J., Martin, S. T., and Bertram, A. K.: Relative humidity-dependent viscosities of isoprene-derived secondary organic material and atmospheric implications for isoprene-dominant forests, Atmos. Chem. Phys., 15, 5145–5159, https://doi.org/10.5194/acp-15-5145-2015, 2015.

Song, M., Liu, P. F., Hanna, S. J., Zaveri, R. A., Potter, K., You, Y., Martin, S. T., and Bertram, A. K.: Relative humidity-dependent viscosity of secondary organic material from toluene photo-oxidation and possible implications for organic particulate matter over megacities, Atmos. Chem. Phys., 16, 8817–8830, https://doi.org/10.5194/acp-16-8817-2016, 2016.

Song, M., Maclean, A. M., Huang, Y., Smith, N. R., Blair, S. L., Laskin, J., Laskin, A., DeRieux, W.-S. W., Li, Y., Shiraiwa, M., Nizkorodov, S. A., and Bertram, A. K.: Liquid–liquid phase separation and viscosity within secondary organic aerosol generated from diesel fuel vapors, Atmos. Chem. Phys., 19, 12515–12529, https://doi.org/10.5194/acp-19-12515-2019, 2019.

Song, Y.-C., Haddrell, A. E., Bzdek, B. R., Reid, J. P., Bannan, T., Topping, D. O., Percival, C., and Cai, C.: Measurements and predictions of binary component aerosol particle viscosity, J. Phys. Chem. A, 120, 8123–8137, https://doi.org/10.1021/acs.jpca.6b07835, 2016.

Song, Y.-C., Lilek, J., Lee, J. B., Chan, M. N., Wu, Z., Zuend, A., and Song, M.: Viscosity and phase state of aerosol particles consisting of sucrose mixed with inorganic salts, Atmos. Chem. Phys., 21, 10215–10228, https://doi.org/10.5194/acp-21-10215-2021, 2021.

Steimer, S. S., Berkemeier, T., Gilgen, A., Krieger, U. K., Peter, T., Shiraiwa, M., and Ammann, M.: Shikimic acid ozonolysis kinetics of the transition from liquid aqueous solution to highly viscous glass, Phys. Chem. Chem. Phys., 17, 31101–31109, https://doi.org/10.1039/C5CP04544D, 2015.

Tong, Y.-K., Liu, Y., Meng, X., Wang, J., Zhao, D., Wu, Z., and Ye, A.: The relative humidity-dependent viscosity of single quasi aerosol particles and possible implications for atmospheric aerosol chemistry, Phys. Chem. Chem. Phys., 24, 10514–10523, https://doi.org/10.1039/D2CP00740A, 2022.

Virtanen, A., Joutsensaari, J., Koop, T., Kannosto, J., Yli-Pirilä, P., Leskinen, J., Mäkelä, J. M., Holopainen, J. K., Pöschl, U., and Kulmala, M.: An amorphous solid state of biogenic secondary organic aerosol particles, Nature, 467, 824–827, https://doi.org/10.1038/nature09455, 2010.

Wang, G., Zhang, R., Gomez, M. E., Yang, L., Zamora, M. L., Hu, M., Lin, Y., Peng, J., Guo, S., and Meng, J.: Persistent sulfate formation from London Fog to Chinese haze, P. Natl. Acad. Sci. USA, 113, 13630–13635, https://doi.org/10.1073/pnas.1616540113, 2016.

Winston, P. W. and Bates, D. H.: Saturated solutions for the control of humidity in biological research, Ecology, 41, 232–237, https://doi.org/10.2307/1931961, 1960.

Xiao, Z.-M., Zhang, Y.-F., Hong, S.-M., Bi, X.-H., Jiao, L., Feng, Y.-C., and Wang, Y.-Q.: Estimation of the main factors influencing haze, based on a long-term monitoring campaign in Hangzhou, China, Aerosol Air Qual. Res., 11, 873–882, https://doi.org/10.4209/aaqr.2011.04.0052, 2011.

Xu, R., Lam, H. K., Wilson, K. R., Davies, J. F., Song, M., Li, W., Tse, Y.-L. S., and Chan, M. N.: Effect of inorganic-to-organic mass ratio on the heterogeneous OH reaction rates of erythritol: implications for atmospheric chemical stability of 2-methyltetrols, Atmos. Chem. Phys., 20, 3879–3893, https://doi.org/10.5194/acp-20-3879-2020, 2020.

Yeung, M. C., Lee, A. K., and Chan, C. K.: Phase transition and hygroscopic properties of internally mixed ammonium sulfate and adipic acid (AS-AA) particles by optical microscopic imaging and Raman spectroscopy, Aerosol Sci. Tech., 43, 387–399, https://doi.org/10.1080/02786820802672904, 2009.

Yli-Juuti, T., Pajunoja, A., Tikkanen, O. P., Buchholz, A., Faiola, C., Väisänen, O., Hao, L., Kari, E., Peräkylä, O., and Garmash, O.: Factors controlling the evaporation of secondary organic aerosol from α-pinene ozonolysis, Geophys. Res. Lett., 44, 2562–2570, https://doi.org/10.1002/2016GL072364, 2017.

Zhang, Q., Jimenez, J. L., Canagaratna, M., Allan, J., Coe, H., Ulbrich, I., Alfarra, M., Takami, A., Middlebrook, A., and Sun, Y.: Ubiquity and dominance of oxygenated species in organic aerosols in anthropogenically-influenced Northern Hemisphere midlatitudes, Geophys. Res. Lett., 34, L13801, https://doi.org/10.1029/2007GL029979, 2007.

Zhang, R., Wang, G., Guo, S., Zamora, M. L., Ying, Q., Lin, Y., Wang, W., Hu, M., and Wang, Y.: Formation of urban fine particulate matter, Chem. Rev., 115, 3803–3855, 2015.

Zobrist, B., Marcolli, C., Pedernera, D., and Koop, T.: Do atmospheric aerosols form glasses?, Atmos. Chem. Phys., 8, 5221–5244, 2008.

Zuend, A. and Seinfeld, J. H.: Modeling the gas-particle partitioning of secondary organic aerosol: the importance of liquid-liquid phase separation, Atmos. Chem. Phys., 12, 3857–3882, https://doi.org/10.5194/acp-12-3857-2012, 2012.

Zuend, A., Marcolli, C., Luo, B. P., and Peter, T.: A thermodynamic model of mixed organic-inorganic aerosols to predict activity coefficients, Atmos. Chem. Phys., 8, 4559–4593, https://doi.org/10.5194/acp-8-4559-2008, 2008.

Zuend, A., Marcolli, C., Booth, A. M., Lienhard, D. M., Soonsin, V., Krieger, U. K., Topping, D. O., McFiggans, G., Peter, T., and Seinfeld, J. H.: New and extended parameterization of the thermodynamic model AIOMFAC: calculation of activity coefficients for organic-inorganic mixtures containing carboxyl, hydroxyl, carbonyl, ether, ester, alkenyl, alkyl, and aromatic functional groups, Atmos. Chem. Phys., 11, 9155–9206, https://doi.org/10.5194/acp-11-9155-2011, 2011.